LANGMUIR

pubs.acs.org/Langmuir Article

Extreme Gradient Boosting to Predict Atomic Layer Deposition for Platinum Nano-Film Coating

Sung-Ho Yoon, Jun-Hyeok Jeon, Seung-Beom Cho, Edric John Cruz Nacpil,* Il Jeon,* Jae-Boong Choi,* and Hyeongkeun Kim*

Cite This: *Langmuir* 2023, 39, 4984–4992 Read Online

ACCESS | Metrics & More | Article Recommendations

ABSTRACT: Extreme gradient boosting (XGBoost) is an artificial intelligence algorithm capable of high accuracy and low inference time. The current study applies this XGBoost to the production of platinum nano-film coating through atomic layer deposition (ALD). In order to generate a database for model development, platinum is coated on α-Al2O3 using a rotary-type ALD equipment. The process is controlled by four parameters: process temperature, stop valve time, precursor pulse time, and reactant pulse time. A total of 625 samples according to different process conditions are obtained. The ALD coating index is used as the Al/Pt component ratio through ICP-AES analysis during postprocessing. The four process parameters serve as the input data and produces the Al/Pt component ratio as the output data. The postprocessed data set is randomly divided into 500 training samples and 125 test samples. XGBoost demonstrates 99.9% accuracy and a coefficient of determination of 0.99. The inference time is lower than that of random forest regression, in addition to a higher prediction safety than that of the light gradient boosting machine.

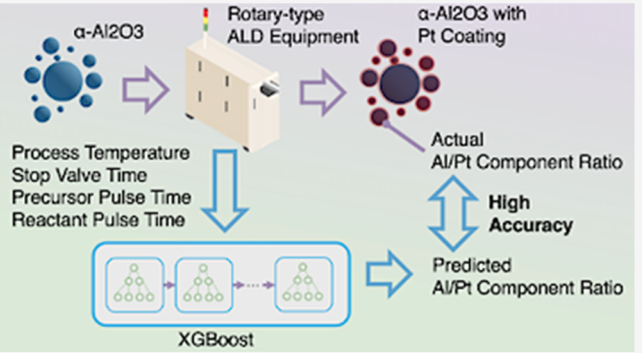

1. INTRODUCTION

Nano/micro particles (NMP)[1−4] constitute new materials for dynamic random-access memory (DRAM)[5−7] and central processing units (CPU).[8−10] The properties of NMPs are mainly determined by size, shape, and composition.[11] In the case of composite NMPs with metal−support interaction (MSI), an interaction between the main component of the particles and the support consisting of the nucleus and the metal surrounding the nucleus has the greatest influence on the properties of NMPs.[12−15] Generally, MSIs include charge transfer,[16−19] interfacial boundary,[20−22] morphology of NMPs,[23−25] chemical composition,[26−28] and strong metal support interaction.[29−31] Therefore, studies have been reported to solve the stability of the support while improving electrical properties of the metal catalyst by coating the existing performance stabilized support with a metal serving as a catalyst.[11] Applying NMPs to cutting-edge information and communication technologies, such as DRAMs and CPUs, motivates efforts to increase the resolution of the processing equipment from micrometers to nanometers. The chemical vapor deposition (CVD) methods, namely, atmosphere pressure CVD, high-density plasma CVD, and atomic layer deposition (ALD), having better process resolution than a physical vapor deposition-based process such as E-beam, sputter, or similar methods, have consequently garnered attention. Since the ALD method is the only CVD method that has a unique advantage of angstrom-level thickness control, as opposed to other thin film deposition processes,[32−34] ALD enables the most conformal and uniform nano-scale thin film process. Conventional ALD equipment absorbs reaction gas using a two-dimensional (2D) substrate in a vacuum, thereby forming a nano-thin film through ALD cycles. On the other hand, since three-dimensional (3D) substrates, namely, NMPs, have significantly higher specific surfaces compared to 2D substrates, initial adsorption is difficult and NMPs are likely to be lost during the process due to the flow field of the reaction gas. Therefore, studies have been actively conducted on advanced rotary-type ALDs,[35−37] fluidized bed-type ALD[38−41] development, and modified ALD processing methods for 3D substrates. Nevertheless, since the ALD process of NMPs has variable processing parameters, namely, sufficient stirring of NMPs, sufficient processing temperature, and the flow field of reaction gas, it is difficult

Received: December 27, 2022
Revised: February 24, 2023
Published: March 22, 2023

ACS Publications

© 2023 The Authors. Published by American Chemical Society

to optimize the ALD process for conformal and uniform coating on the vast specific surfaces of NMPs. In particular, a long reaction time is required to coat a large surface area of NMPs with metal or metal oxide through an ALD process. Therefore, the coating process is modified by the stop valve time as an additional process step to secure the reaction time. This step closes all valves between the pulse and purge step of the reaction.[38−41] The process was successful, although the process time increased due to the additional process step. Thus, process optimization is required.

In the interest of optimizing the ALD process, this study proposes a process prediction method that is divided into two stages: data set generation and model development. Using test samples from the experimental data set, we trained and tested our proposed extreme gradient boosting (XGBoost),[42] linear regression, random forests regression (RFR),[43] and light gradient boosting machine (LGBM).[44] We evaluated the models using root mean square error (RMSE) value and the coefficient of determination value (R^2 score).

The major contributions of the current study are as follows:

1. The XGBoost model predicted ALD coating results more accurately than the other regression models.
2. We verified that the four processing parameters, namely, processing temperature, precursor pulse time, reactant pulse time, and stop valve time, have the most influence on the conformal coating process of the platinum nano-film using a rotary-type ALD.
3. It has been found to be most efficient to use the XGBoost mechanism to predict the outcome of the coating process of the platinum nano-film using a rotary-type ALD through machine learning.

Further details of these contributions are conveyed as follows: Section 2 describes the methodology for the ALD process, machine learning methods, and data set generation. Section 3 presents and discusses the prediction results for the models. Finally, Section 4 provides conclusions based on the results.

2. EXPERIMENTAL SECTION

2.1. Platinum Deposition Process Using Rotary-Type ALD. We used the spherical α-Al2O3 powder (DAM-05, Denka) shown in Figure 1a for the ALD process to minimize extraneous variables in developing machine learning for predicting the platinum nano-film coating process. The coating was formed from a rotary-type ALD (Atomic-Shell ALD, CN1, Hwaseong, Korea) shown in Figure 1b. In this paper, a 300 cm^3 reactor was used along with a mesh filter with 0.3 μm pores at the end of the reactor to prevent the loss of 5.0 μm α-Al2O3 powder shown in Figure 1c,d. We performed the ALD process for the nano-film coating using MeCpPtMe3, that is, platinum as a precursor gas, oxygen as a reactant gas, and nitrogen as a purge gas. In order to increase the amount of pulsed platinum, the temperature of the bubbler-type canister is heated to 80 °C, while 50 sccm of argon gas is used as a carrier gas. Advanced ALD with a stop valve mode was applied to coat platinum nano-films onto the α-Al2O3 powder with a large specific surface area. Since catalyst performance was determined by the amount of platinum deposited on the micro-sized powder, it was necessary to quantify the amount of coated platinum. The amount of coated platinum was quantified using an inductively coupled plasma-atomic emission spectroscopy (ICP-AES) equipment (Optima-4300 DV, PerkinElmer). When the platinum-coated α-Al2O3 powder was exposed to ICP, oxygen was completely decomposed. Since only two components of aluminum and platinum remained inside the ICP-AES equipment, we were able to measure the amount of coated platinum nano-films relative to the existing α-Al2O3 powder quantified as the atomic component ratio of Pt/Al.

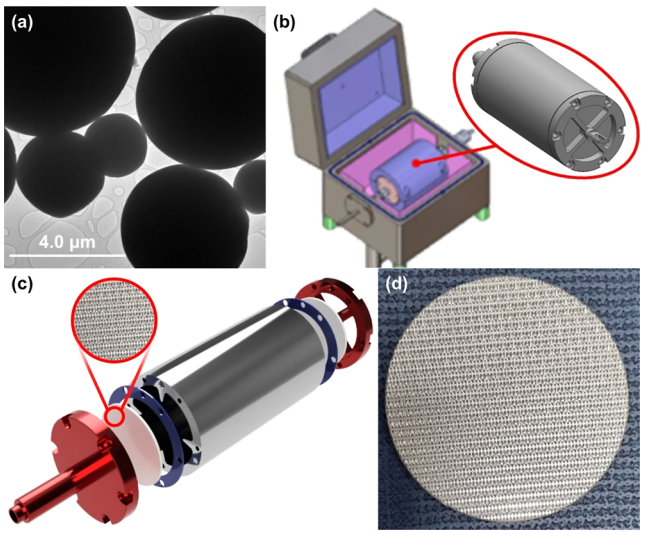

Figure 1. 3D modeling of rotary-type ALD equipment and Al2O3 powder for platinum nano-film coating. (a) TEM image of spherical α-Al2O3 powder. (b) 3D modeling of rotary-type ALD process chamber and reactor. (c) Assembled reactor. (d) Mesh filter to prevent powder loss.

2.2. Processing Parameters for ALD of Platinum. A normal ALD technique shown in Figure 2a has a cycle consisting of four steps: precursor pulse, precursor purge, reactant pulse, and reactant purge. In the case of a 2D substrate such as a Si wafer with a small specific surface area, the reaction time for ligand exchange is sufficient even with the normal ALD process, where there is a brief contact time between the precursor or reactant and the reaction surface of the substrate. However, in the case of a 3D substrate with a large specific surface area such as micro-size powder, the time for reactants and precursors to react with the reaction surface of the powder is insufficient. In this paper, a stop valve step is added to allow sufficient reaction time by locking all valves between the pulse and purge steps of the reaction gases. This process cycle is the advanced ALD technique shown in Figure 2b. Processing parameters affecting the amount of platinum nano-film deposited on α-Al2O3 powder under various processing conditions of advanced ALD were evaluated as follows:

The Pt/Al ratio of the platinum nano-film was calculated according to the stop valve time with a fixed processing temperature of 300 °C, a platinum pulse time of 0.5 s, and an O2 pulse time of 5.0 s. During stop valve activation, the platinum nano-film was coated on α-Al2O3 powder. As the activation time increased from 5.0 to 25.0 s, the Pt/Al component ratio increased from 0.545 to 0.750%, as shown in Figure 2c.

1. The Pt/Al ratio was calculated relative to the processing temperature with a fixed stop valve time of 5.0 s, platinum pulse time of 0.5 s, and an O2 pulse time of 5.0 s. As the processing temperature increased from 200 to 400 °C, the Pt/Al component ratio increased from approximately 0.031−0.544%, as shown in Figure 2d.
2. The Pt/Al ratio of the platinum nano-film was calculated according to the platinum pulse time with a fixed stop valve time of 5.0 s, a processing temperature of 300 °C, and an O2 pulse time of 5.0 s. As the platinum pulse time was changed from 0.5 to 2.5 s, the Pt/Al component ratio increased from approximately 0.318−1.677% (Figure 2e).
3. The Pt/Al ratio of the platinum nano-film was calculated relative to the O2 pulse time with a fixed stop valve time of 5.0 s, processing temperature of 300 °C, and platinum pulse time of 0.5 s. As the O2 pulse time was changed from 5.0 to 25.0 s, the ratio increased from approximately 0.186−0.616%, as shown in Figure 2f.

https://doi.org/10.1021/acs.langmuir.2c03465
Langmuir 2023, 39, 4984−4992

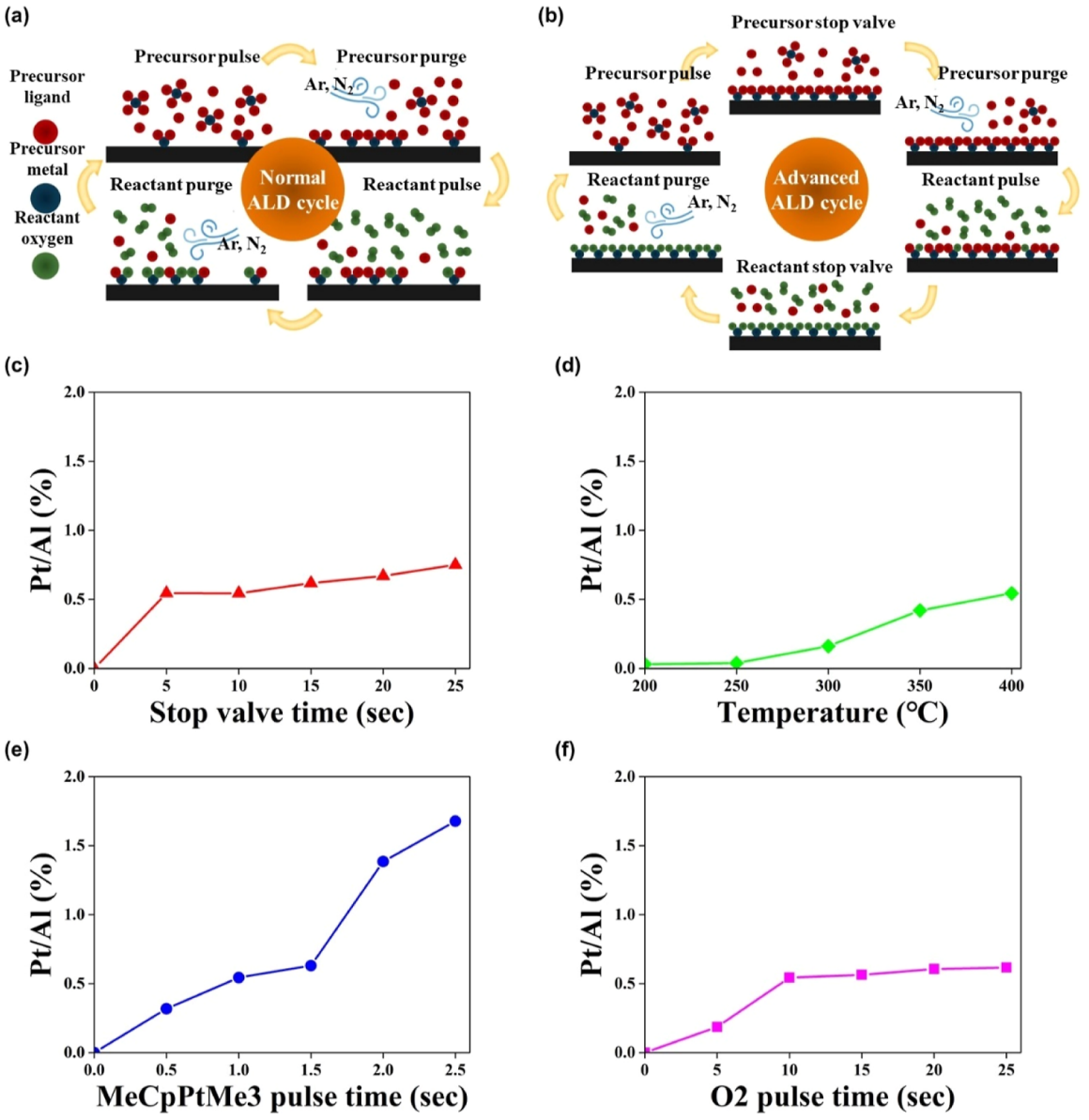

Figure 2. Difference between normal ALD technique and advanced ALD technique and ICP-AES analysis of rotary-type ALD platinum nano-film on α-Al2O3 powder for four processing parameters. (a) Schematic of normal ALD cycle, (b) schematic of advanced ALD cycle, (c) atomic component ratio of the Pt/Al element under different stop valve times, (d) atomic component ratio of the Pt/Al element under different processing temperatures, (e) atomic component ratio of the Pt/Al element under different MeCpPtMe3 pulse times, and (f) atomic component ratio of Pt/Al element under different O2 pulse times.

We therefore defined four processing parameters, namely, stop valve time, processing temperature, platinum pulse time, and O2 pulse time, as factors determining the amount of the platinum nano-film coated on α-Al2O3 powder.

2.3. Machine Learning Models for Platinum Nano-Film Growth Prediction. As discussed in Section 2.1, traditional methods for analyzing the deposition amount of nano-thin films of powder include photographic methods using a transmission electron microscope, X-ray analysis such as X-ray fluorescence, and component ratio analysis method using plasma, such as ICP-AES. Therefore, we used machine learning as a method to increase predictive power, while preventing the problem of multicollinearity of variables due to the multivariable characteristics of the ALD process.

Machine learning is defined as understanding the structure of data by analyzing and learning data based on algorithms by computers to predict results.[41] Therefore, machine learning is sometimes useful, but it is difficult to mathematically derive models because the data is too vast and complex for humans to sufficiently comprehend. Nevertheless, humans may select machine learning methods based on the structure of the data. Since the ALD process results in the current study are not purely linear in relation to our four processing variables, it is suitable to use a nonlinear, non-parametric model. Whereas a parametric model is a probability distribution group that can be explained by mobilizing finite parameters, where k-dimensional parameter vector, the non-parametric model has a parametric space with infinite dimensions. It is assumed that the coupling form of the parameters is linear or non-linear, without making special assumptions. Representative non-parametric models include general additive modeling; decision tree-based methods, as shown in Figure 3a; polynomial regression modeling; support vector machines; and multivariate adaptive regression spline methods.[41] The decision tree-based model is widely used because it is simple and human interpretable and can be readily expressed using diagrams. Although such modeling is known for low accuracy, random forests use thousands of trees to improve performance. More recent XGBoost implementations and LGBMs build upon this advancement by

https://doi.org/10.1021/acs.langmuir.2c03465
Langmuir 2023, 39, 4984−4992

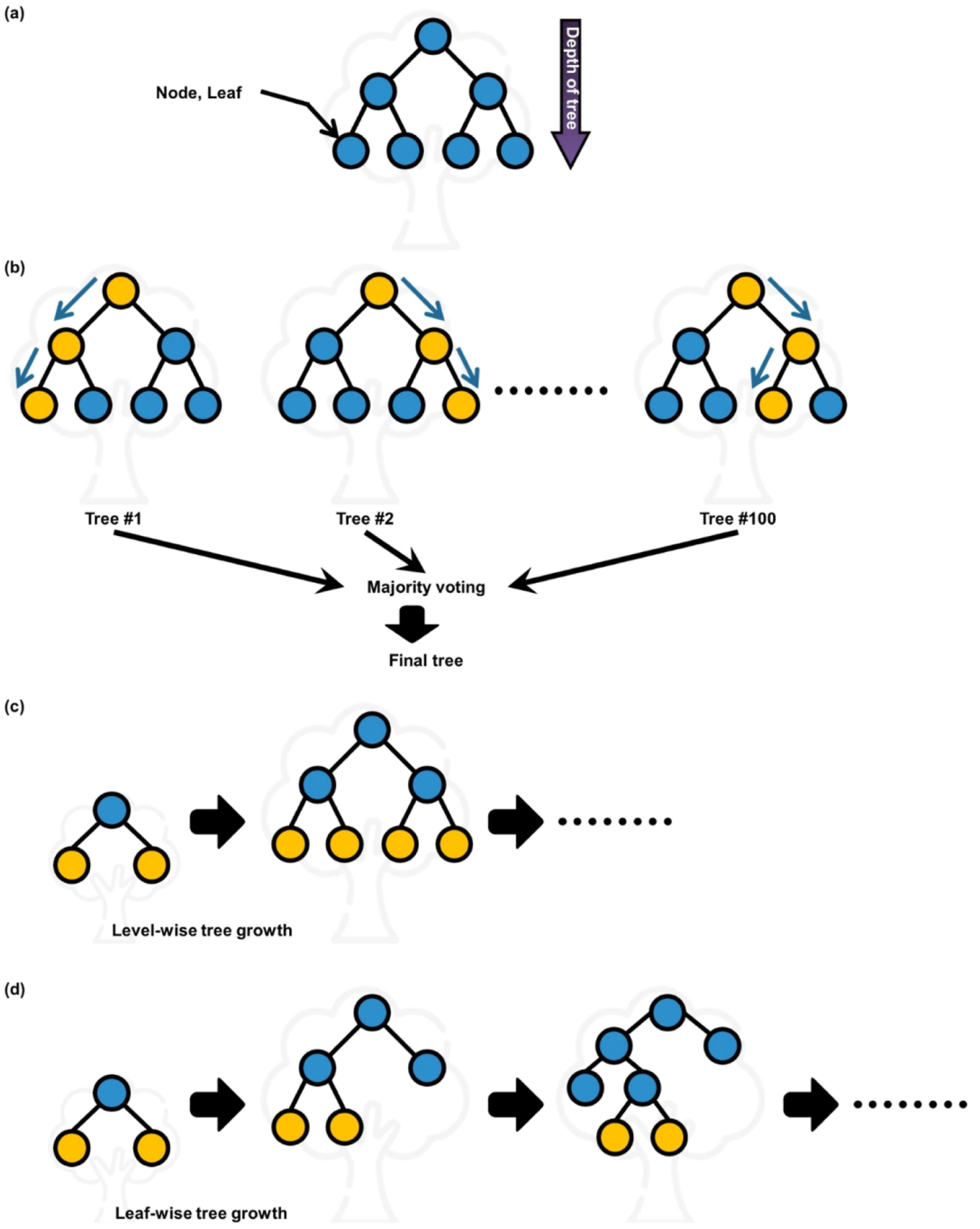

Figure 3. Regression algorithms for machine learning. (a) Decision tree, (b) RFR, (c) XGBoost regression, and (d) LGBM regression.

addressing the problems of overfitting regulation and high inference time encountered by other algorithms. Hence, the prediction accuracy of our Pt-ALD coating process is analyzed using the following methods, along with linear regression and random forest models.

1. Random forest is a machine learning algorithm that selects variables having a strong causal relationship with the dependent variable among multiple independent variables. Although it is impossible to present a final model, random forest has the advantage of excellent performance in all aspects of classification and regression. The random forest algorithm is a method that combines the decision tree-based method and the ensemble technique. This method is an algorithm that finds the decision tree with the best predictive power among n decision trees, as shown in Figure 3b.
2. XGBoost and LGBM have been reported in recent studies for their excellent predictive power and low inference time. Boosting derives an ensemble with excellent performance by sequentially learning models with weak predictive power. When the model is integrated with the boosting method, the nth weight is given according to the error of the n-1st model, and the objective function is composed of a regularization term representing the model complexity and loss function between the predicted value and the true value. However, the difference between XGBoost and LGBM is the growth direction of the decision tree. When growing a tree as large as layer $n - 1$ to layer n, XGBoost calculates only the weight, while saving all the branches of the tree as shown in Figure 3C. Conversely, LGBM removes the branches with less weight to grow into new layers as shown in Figure 3d. For this reason, XGBoost is called level-wise tree growth, whereas LGBM is called leaf-wise

https://doi.org/10.1021/acs.langmuir.2c03465
Langmuir 2023, 39, 4984−4992

tree growth. Therefore, XGBoost and LGBM are methods to improve the error of the preceding tree by sequentially learning the decision tree. Compared to other decision tree-based models, they have high scalability and fast processing speed, along with the advantage of simple data pre-processing.

2.4. Machine Learning Data Set. As discussed in Section 2.2, the amount of platinum nano-film coated on α-Al2O3 powder is determined by four parameters. Prediction of the proposed rotary-type ALD is made on a total of 625 samples. The samples contain five cases each of four parameters:

1. Stop valve time from 5.0 to 25.0 s
2. Processing temperature from 200 to 400 °C
3. Platinum pulse time from 0.5 to 2.5 s
4. O2 pulse time from 5.0 to 25.0 s

80% of the total of 625 samples was used for training, whereas the remaining 20% of the data set was used as a test data set for evaluation, as denoted in Table 1.

Table 1. RSME Values and R^2 Score of Machine Learning Models

	training		test	
model of machine learning	RMSE	R^2 score	RMSE	R^2 score
linear regression	0.25144	0.774	0.26987	0.719
RFR	0.01194	0.999	0.04547	0.991
XGBoost	0.02958	0.997	0.03190	0.996
LGBM	0.02659	0.998	0.03450	0.995

3. RESULTS AND DISCUSSION

The prediction accuracy of the proposed modeling method was assessed through two indicators: RMSE and R^2 score. RMSE is the root of the average squared difference between the predicted value of the model and the experimental value as follows

$$\text{root mean square error (RMSE)} = \sqrt{\frac{1}{n}\sum_{i=1}^{n}(x_i - y_i)^2} \quad (1)$$

where y_i is the experimental value and x_i is the predicted value. Since the difference is squared, the RSME does not explicitly indicate whether the model is underestimating or overestimating. On the other hand, the R^2 score is a value that quantifies the degree of influence between variables or the degree of causal relationship. The higher the coefficient of determination, the better the independent variable explains the dependent variable. The R^2 score has a range between 0 and 1, with the fit of the model improving as the score approaches 1. The R^2 score is calculated as follows

$$\begin{aligned}&\text{coefficient of determination } (R^2 \text{ score})\\ &= \text{SSE/SST}\\ &= 1 - \text{SSR/SST}\end{aligned} \quad (2)$$

where SST is the sum of the total squares of the differences between the experimental value and the mean of the experimental values, SSE is the sum of regression squares of the differences between the regression model predictions value and the mean of experimental values, and SSR is the sum of squared residuals of the differences between the experimental values and the predicted values of the regression model as follows

$$\text{SST} = \sum_{i=1}^{n}(x_i - \overline{x_i})^2 \quad (3)$$

$$\text{SSE} = \sum_{i=1}^{n}(y_i - \overline{x_i})^2 \quad (4)$$

$$\text{SSR} = \sum_{i=1}^{n}(x_i - y_i)^2 \quad (5)$$

R^2 scores and RMSEs are shown in Table 1.

3.1. Linear Regression. A linear regression model was used as a representative of non-decision tree-based regression. The parameters of the linear regression model having a significant effect on model learning were the fit intercept and the normalization. Linear regression model training was carried out by setting the true value of the fit intercept and deprecated normalization. Therefore, the linear regression model used was one without intercept and normalization.

Training data predictions had an RMSE value of 0.25114 and an R^2 score of 0.774. On the other hand, the test data predictions had an RMSE value of 0.26987 and an R^2 score of 0.719. The distribution plot of the predicted values shown in Figure 4 confirmed that the distribution had a large area, and therefore, the differences between the actual values and the predicted values were significant.

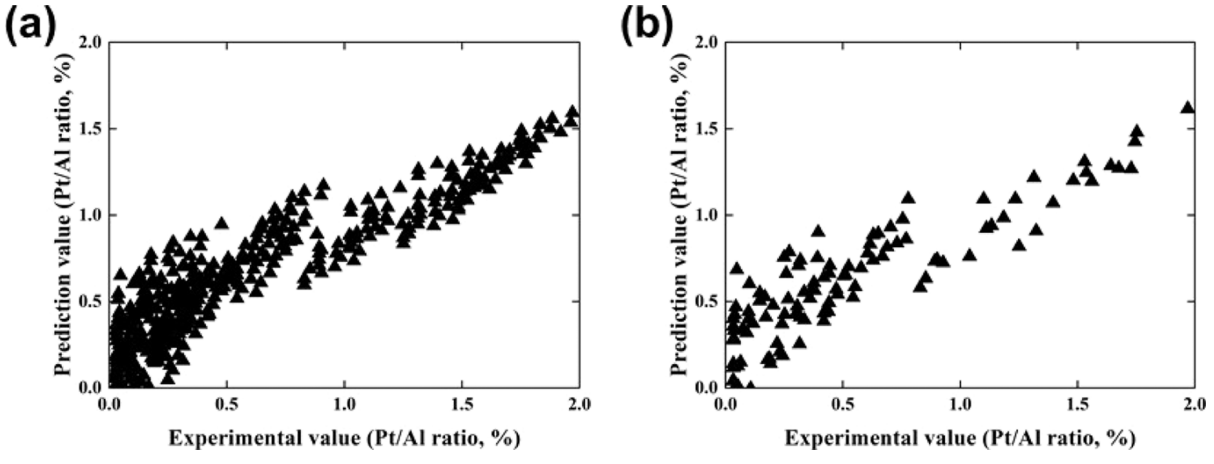

Figure 4. Distribution plot of predicted values from linear regression model. (a) Training data. (b) Test data.

https://doi.org/10.1021/acs.langmuir.2c03465
Langmuir 2023, 39, 4984−4992

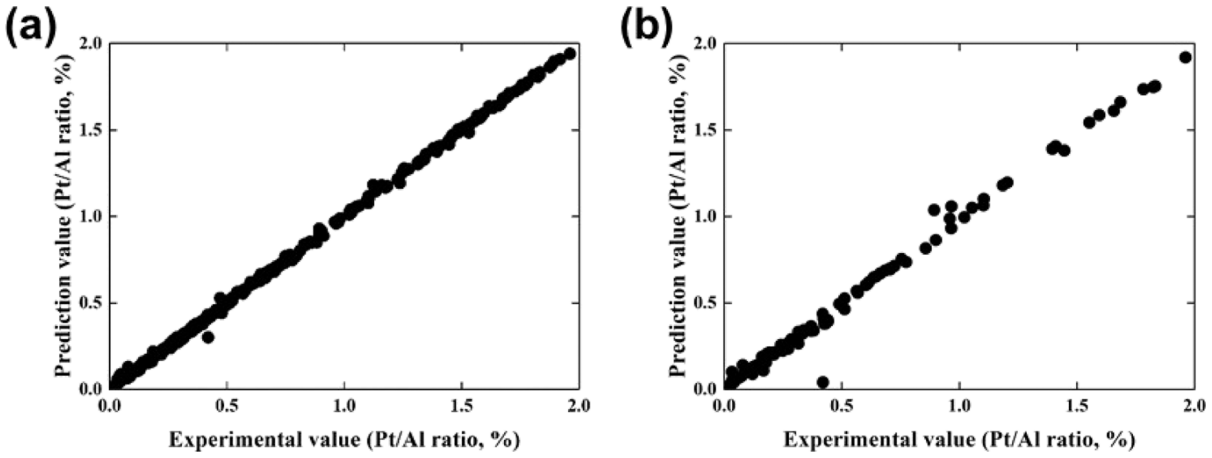

Figure 5. Distribution plot of predicted values from RFR model. (a) Training data. (b) Test data.

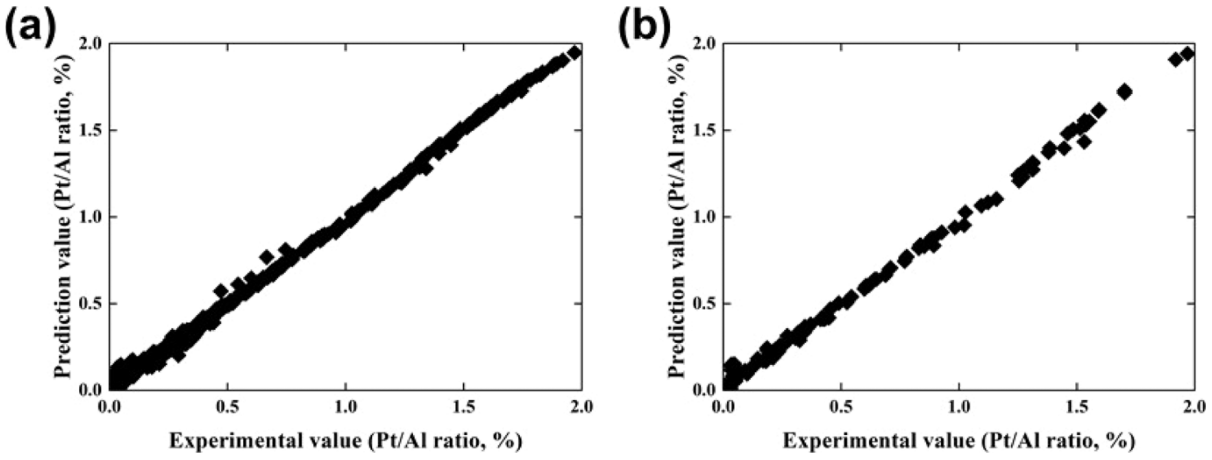

Figure 6. Distribution plot of predicted values from XGBoost model. (a) Training data. (b) Test data.

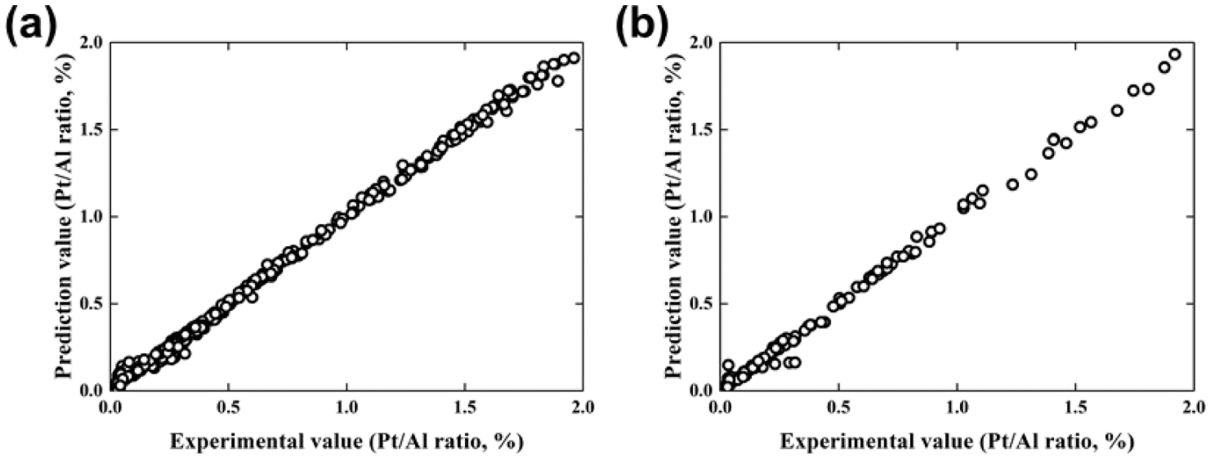

Figure 7. Distribution plot of predicted values in LGBM model. (a) Training data. (b) Test data.

3.2. Linear Forest. The random forest model is an ensemble model of decision tree-based regression. The model parameters having a significant effect on learning are the number of trees and the maximum depth. Model training was performed for 100 trees and without setting the maximum depth. The nodes thus expanded indefinitely until the optimal result was obtained. Training had an RMSE value of 0.01194 and an R^2 score of 0.999. On the other hand, testing had an RMSE value of 0.04547 and an R^2 score of 0.991. The distribution plot of the predicted values in Figure 5 indicates an insignificant difference between the actual and predicted values.

3.3. EXtreme Gradient Boosting. The XGBoost model is a level-wise tree growth model of decision tree-based regression. Model parameters having a significant effect on learning are the number of trees, maximum depth, and learning rate. Model training was carried out by specifying 100 trees, a maximum depth of 3, and a learning rate of 0.1. The accuracy

https://doi.org/10.1021/acs.langmuir.2c03465
Langmuir 2023, 39, 4984−4992

of the model is expressed by the RMSE value and the R^2 score. Training the model yielded an RMSE of 0.02958 and an R^2 score of 0.997, whereas an RMSE value of 0.03190 and an R^2 score of 0.996 were achieved on the test data set. Note that the distribution plot of the predicted values in Figure 6 shows an insignificant difference between predicted and experimental values.

3.4. Light Gradient Boosting Machine. The LGBM is a leaf-wise tree growth model of decision tree-based regression. The parameters of the LGBM model having a significant influence on model learning are the number of trees, maximum tree leaves, and learning rate. 100 trees were set up for training, with maximum tree leaves being 31 and a learning rate of 0.1. An RMSE value of 0.02659 and an R^2 score of 0.998 resulted from training. Testing had an RMSE value of 0.03450 and an R^2 score of 0.995. The distribution plot of the predicted values in Figure 7 shows that the difference between the actual and predicted values is insignificant.

4. CONCLUSIONS

The AI approach XGBoost was optimized to predict advanced ALD process results with 99.9% accuracy and an R^2 score of 0.99. Although a traditional nano/micro-particle analysis system takes 150 days to secure the process results through actual experiments and ICP-AES analysis for 125 test samples, machine learning using forest-based models, such as random forest, XGBoost, and LGBM, takes only tens of seconds. As shown in Table 1, the linear regression model cannot accurately predict the process, as indicated by an R^2 score of 0.77 for both the training and test data. However, for all forest-based models, the R^2 score of the training data and the test data is higher than 0.99. The random forest model shows the highest accuracy among the training data, although test results have the lowest accuracy. In contrast, XGBoost and LGBM show higher accuracy in the prediction of test data. In the case of random forest and linear regression, the most suitable model is found among random weight functions to predict new data. Therefore, finding a combination of accurately predictive weight functions is nearly random due to the limitation of the small experimental database size of 625. On the other hand, XGBoost and LGBM assign a value to the weight function so that the model grows and predicts more accurately than the previous layer. Since the optimized combination of weight functions is calculated, it is possible to predict with high accuracy, even with a small experimental database size of 625. XGBoost is an algorithm with stronger prediction accuracy, whereas LGBM generally has a lower inference time with a larger database. Thus, LGBM showed unstable results, since the 625 experimental data points did not meet the general recommended data amount of 10,000 for leaf-wise growth. The XGBoost model consequently has the highest and most stable prediction accuracy across multiple variables.

Our study is limited to four process conditions. If it is possible to obtain more experimental data, it will be possible to predict the process results for more process conditions and sudden process changes such as human error. In addition, predictions through algorithms that require large databases such as LGBM are expected to be feasible.

The proposed approach transcends the current study with the potential to solve various engineering problems regarding nano/micro-structures, particles, and multivariate processes. Possible future applications include various industries such as automobiles, semiconductors, and energy.

AUTHOR INFORMATION

Corresponding Authors

Edric John Cruz Nacpil − *Department of Nano Engineering, Department of Nano Science and Technology, SKKU Advanced Institute of Nanotechnology (SAINT), Sungkyunkwan University (SKKU), Suwon, Gyeonggi-do 16419, Republic of Korea*; Email: edricjohnnacpil@gmail.com

Il Jeon − *Department of Nano Engineering, Department of Nano Science and Technology, SKKU Advanced Institute of Nanotechnology (SAINT), Sungkyunkwan University (SKKU), Suwon, Gyeonggi-do 16419, Republic of Korea*; orcid.org/0000-0002-4220-8374; Email: il.jeon@spc.oxon.org

Jae-Boong Choi − *Mechanical Engineering, Sungkyunkwan University, Suwon, Gyeonggi-do 16419, Republic of Korea*; Email: boong33@skku.edu

Hyeongkeun Kim − *Electronic Convergence Materials and Device Research Center, Korea Electronics Technology Institute, Seongnam 13509, Republic of Korea*; orcid.org/0000-0002-7875-8853; Email: faithkim99@keti.re.kr

Authors

Sung-Ho Yoon − *Electronic Convergence Materials and Device Research Center, Korea Electronics Technology Institute, Seongnam 13509, Republic of Korea; Mechanical Engineering, Sungkyunkwan University, Suwon, Gyeonggi-do 16419, Republic of Korea; Department of Nano Engineering, Department of Nano Science and Technology, SKKU Advanced Institute of Nanotechnology (SAINT), Sungkyunkwan University (SKKU), Suwon, Gyeonggi-do 16419, Republic of Korea*

Jun-Hyeok Jeon − *Electronic Convergence Materials and Device Research Center, Korea Electronics Technology Institute, Seongnam 13509, Republic of Korea; Mechanical Engineering, Sungkyunkwan University, Suwon, Gyeonggi-do 16419, Republic of Korea*

Seung-Beom Cho − *Mechanical Engineering, Sungkyunkwan University, Suwon, Gyeonggi-do 16419, Republic of Korea*

Complete contact information is available at: https://pubs.acs.org/10.1021/acs.langmuir.2c03465

Notes

The authors declare no competing financial interest.

ACKNOWLEDGMENTS

S.-H Yoon and J.-H. Jeon contributed equally to this work. This study was supported by the Research Program funded by the Seoul National University of Science and Technology. Characterization was acquired from the Research Institute of Advanced Materials (RIAM) in Seoul National University. This work was supported by TIPA funded by the ministry of SMEs (S3177448). This work was also supported by the National Research Foundation of Korea funded by the Ministry of Science and ICT (MSIT), Korea (NRF-2020M3H4A3081879, NRF-2021R1C1C1009200). This work was supported by the Postdoctoral Research Program of Sungkyunkwan University (2022).

REFERENCES

(1) Sun, J.; Zhao, J.; Chen, Y.; Wang, L.; Yun, X.; Huang, Z. Macro-Micro-Nano Multistage Toughening in Nano-Laminated Graphene Ceramic Composites. *Mater. Today Phys.* **2022**, *22*, 100595.

(2) Mahdi Rafiee, M.; Baniassadi, M.; Wang, K.; Baniasadi, M.; Baghani, M. Mechanical Properties Improvement of Shape Memory Polymers by Designing the Microstructure of Multi-Phase Heterogeneous Materials. *Comput. Mater. Sci.* **2021**, *196*, 110523.
(3) Wang, Y.; Zhang, D.; Yang, Y.; Guo, Y.; Bai, Z.; Chu, P. K.; Luo, Y. Three-Dimensional Nano/Micro-Structured Porous MoP/CNTs Microspheres as High-Capacity Anode for Lithium-Ion Batteries. *J. Alloys Compd.* **2021**, *872*, 159608.
(4) Li, X.; Yang, X.; Yi, D.; Liu, B.; Zhu, J.; Li, J.; Gao, C.; Wang, L. Effects of NbC Content on Microstructural Evolution and Mechanical Properties of Laser Cladded Fe50Mn30Co10Cr10-XNbC Composite Coatings. *Intermetallics* **2021**, *138*, 107309.
(5) Liu, S.; Kappes, B. B.; Amin-ahmadi, B.; Benafan, O.; Zhang, X.; Stebner, A. P. Physics-Informed Machine Learning for Composition−Process−Property Design: Shape Memory Alloy Demonstration. *Appl. Mater. Today* **2021**, *22*, 100898.
(6) Shao, Y.; Hu, W.; Gao, M.; Xiao, Y.; Huang, T.; Zhang, N.; Yang, J.; Qi, X.; Wang, Y. Flexible MXene-Coated Melamine Foam Based Phase Change Material Composites for Integrated Solar-Thermal Energy Conversion/Storage, Shape Memory and Thermal Therapy Functions. *Compos. Appl. Sci. Manuf.* **2021**, *143*, 106291.
(7) Fang, W.; Song, S.; Zhao, J.; Li, C.; Cai, D.; Song, Z. Outstanding Phase-Change Behaviors of GaGeSbTe Material for Phase-Change Memory Application. *Mater. Res. Bull.* **2022**, *149*, 111731.
(8) Mohammed, M.; Wilson, D.; Gomez-Kervin, E.; Petsiuk, A.; Dick, R.; Pearce, J. M. Sustainability and Feasibility Assessment of Distributed E-Waste Recycling Using Additive Manufacturing in a Bi-Continental Context. *Addit. Manuf.* **2022**, *50*, 102548.
(9) Kim, J.; Kim, B. S.; Lee, A. J.; Han, D. H.; Hwang, J. H.; Kim, Y.; Song, K. C.; Oh, H.; Kim, S.; Park, Y.; Jeon, W. Y-Doped HfO2 Deposited by Atomic Layer Deposition Using a Cocktail Precursor for DRAM Capacitor Dielectric Application. *Ceram. Int.* **2022**, *48*, 3236−3242.
(10) van Deelen, T. W.; Hernández Mejía, C.; de Jong, K. P. Control of Metal-Support Interactions in Heterogeneous Catalysts to Enhance Activity and Selectivity. *Nat. Catal.* **2019**, *2*, 955−970.
(11) Prasad, D. H.; Ji, H. I.; Kim, H. R.; Son, J. W.; Kim, B. K.; Lee, H. W.; Lee, J. H. Effect of Nickel Nano-Particle Sintering on Methane Reforming Activity of Ni-CGO Cermet Anodes for Internal Steam Reforming SOFCs. *Appl. Catal., B* **2011**, *101*, 531−539.
(12) Mariño, F.; Baronetti, G.; Jobbagy, M.; Laborde, M. Cu-Ni-K/γ-Al2O3 Supported Catalysts for Ethanol Steam Reforming: Formation of Hydrotalcite-Type Compounds as a Result of Metal−Support Interaction. *Appl. Catal., A* **2003**, *238*, 41−54.
(13) Bernal, S.; Calvino, J. J.; Cauqui, M. A.; Gatica, J. M.; López Cartes, C.; Pérez Omil, J. A.; Pintado, J. M. Some Contributions of Electron Microscopy to the Characterisation of the Strong Metal−Support Interaction Effect. *Catal. Today* **2003**, *77*, 385−406.
(14) Riva, R.; Miessner, H.; Vitali, R.; Del Piero, G. Metal−Support Interaction in Co/SiO2 and Co/TiO2. *Appl. Catal., A* **2000**, *196*, 111−123.
(15) Pacchioni, G.; Freund, H. J. Controlling the Charge State of Supported Nanoparticles in Catalysis: Lessons from Model Systems. *Chem. Soc. Rev.* **2018**, *47*, 8474−8502.
(16) Chen, M. S.; Goodman, D. W. The Structure of Catalytically Active Gold on Titania. *Science* **2004**, *306*, 252−255.
(17) Luches, P.; Pagliuca, F.; Valeri, S.; Illas, F.; Preda, G.; Pacchioni, G. Nature of Ag Islands and Nanoparticles on the CeO2(111) Surface. *J. Phys. Chem. C* **2012**, *116*, 1122−1132.
(18) Pacchioni, G. Electronic Interactions and Charge Transfers of Metal Atoms and Clusters on Oxide Surfaces. *Phys. Chem. Chem. Phys.* **2013**, *15*, 1737−1757.
(19) Molina, L. M.; Hammer, B. Some Recent Theoretical Advances in the Understanding of the Catalytic Activity of Au. *Appl. Catal., A* **2005**, *291*, 21−31.
(20) Zhang, B.; Qin, Y. Interface Tailoring of Heterogeneous Catalysts by Atomic Layer Deposition. *ACS Catal.* **2018**, *8*, 10064−10081.
(21) Lin, X.; Nilius, N.; Sterrer, M.; Koskinen, P.; Häkkinen, H.; Freund, H. J. Characterizing Low-Coordinated Atoms at the Periphery of MgO-Supported Au Islands Using Scanning Tunneling Microscopy and Electronic Structure Calculations. *Phys. Rev. B: Condens. Matter Mater. Phys.* **2010**, *81*, 153406.
(22) Roldan Cuenya, B. Metal Nanoparticle Catalysts Beginning to Shape-Up. *Acc. Chem. Res.* **2013**, *46*, 1682−1691.
(23) Karim, A. M.; Prasad, V.; Mpourmpakis, G.; Lonergan, W. W.; Frenkel, A. I.; Chen, J. G.; Vlachos, D. G. Correlating Particle Size and Shape of Supported Ru/γ-Al2O3 Catalysts with NH3 Decomposition Activity. *J. Am. Chem. Soc.* **2009**, *131*, 12230−12239.
(24) Henry, C. R. Morphology of Supported Nanoparticles. *Prog. Surf. Sci.* **2005**, *80*, 92−116.
(25) Bartholomew, C. H. Mechanisms of Catalyst Deactivation. *Appl. Catal., A* **2001**, *212*, 17−60.
(26) van Deelen, T. W.; Nijhuis, J. J.; Krans, N. A.; Zečević, J.; de Jong, K. P. Preparation of Cobalt Nanocrystals Supported on Metal Oxides To Study Particle Growth in Fischer−Tropsch Catalysts. *ACS Catal.* **2018**, *8*, 10581−10589.
(27) Penner, S.; Armbrüster, M. Formation of Intermetallic Compounds by Reactive Metal−Support Interaction: A Frequently Encountered Phenomenon in Catalysis. *ChemCatChem* **2015**, *7*, 374−392.
(28) Tauster, S. J.; Fung, S. C.; Garten, R. L. Strong Metal-Support Interactions. Group 8 Noble Metals Supported on Titanium Dioxide. *J. Am. Chem. Soc.* **1978**, *100*, 170−175.
(29) Tauster, S. J.; Fung, S. C.; Baker, R. T. K.; Horsley, J. A. Strong Interactions in Supported-Metal Catalysts. *Science* **1981**, *211*, 1121−1125.
(30) Hernández-Cristóbal, O.; Arenas-Alatorre, J.; Díaz, G.; Bahena, D.; Yacamán, M. J. High Resolution HAADF Characterization of Ir/TiO2 Catalyst Reduced at 500 °C: Intensity Profile Analysis. *J. Phys. Chem. C* **2015**, *119*, 11672−11678.
(31) Dasgupta, N. P.; Meng, X.; Elam, J. W.; Martinson, A. B. F. Atomic Layer Deposition of Metal Sulfide Materials. *Acc. Chem. Res.* **2015**, *48*, 341−348.
(32) Wang, G.; Gao, Z.; Tang, S.; Chen, C.; Duan, F.; Zhao, S.; Lin, S.; Feng, Y.; Zhou, L.; Qin, Y. Microwave Absorption Properties of Carbon Nanocoils Coated with Highly Controlled Magnetic Materials by Atomic Layer Deposition. *ACS Nano* **2012**, *6*, 11009−11017.
(33) Peng, Q.; Sun, X. Y.; Spagnola, J. C.; Hyde, G. K.; Spontak, R. J.; Parsons, G. N. Atomic Layer Deposition on Electrospun Polymer Fibers as a Direct Route to Al2O3 Microtubes with Precise Wall Thickness Control. *Nano Lett.* **2007**, *7*, 719−722.
(34) Li, Z.; Su, J.; Wang, X. Atomic Layer Deposition in the Development of Supercapacitor and Lithium-Ion Battery Devices. *Carbon* **2021**, *179*, 299−326.
(35) Kim, J. W.; Kim, D. H.; Oh, D. Y.; Lee, H.; Kim, J. H.; Lee, J. H.; Jung, Y. S. Surface Chemistry of LiNi0.5Mn1.5O4 Particles Coated by Al2O3 Using Atomic Layer Deposition for Lithium-Ion Batteries. *J. Power Sources* **2015**, *274*, 1254−1262.
(36) Jang, E.; Kim, D. W.; Hong, S. H.; Park, Y. M.; Park, T. J. Visible Light-Driven g-C3N4@ZnO Heterojunction Photocatalyst Synthesized via Atomic Layer Deposition with a Specially Designed Rotary Reactor. *Appl. Surf. Sci.* **2019**, *487*, 206−210.
(37) Grillo, F.; Kreutzer, M. T.; van Ommen, J. R. Modeling the Precursor Utilization in Atomic Layer Deposition on Nanostructured Materials in Fluidized Bed Reactors. *Chem. Eng. J.* **2015**, *268*, 384−398.
(38) Wank, J. R.; George, S. M.; Weimer, A. W. Nanocoating Individual Cohesive Boron Nitride Particles in a Fluidized Bed by ALD. *Powder Technol.* **2004**, *142*, 59−69.
(39) King, D. M.; Spencer, J. A.; Liang, X.; Hakim, L. F.; Weimer, A. W. Atomic Layer Deposition on Particles Using a Fluidized Bed Reactor with in Situ Mass Spectrometry. *Surf. Coat. Technol.* **2007**, *201*, 9163−9171.
(40) Bae, S. W. Forecasting Property Prices Using the Machine Learning Methods: Model Comparisons, Ph.D. Dissertation, Depart-

https://doi.org/10.1021/acs.langmuir.2c03465
Langmuir 2023, 39, 4984−4992

ment of Urban Planning and Real Estate, Dankuk University, Seoul, 2019.
(41) Lee, C. R. Estimating Single-Family House Prices Using Non-Parametric Spatial Models and an Ensemble Learning Approach, Ph.D. Dissertation, Department of Geography, Seoul National University, Seoul, 2015.
(42) Chen, T.; Guestrin, C. XGBoost: A Scalable Tree Boosting System. In *Proceedings of the 22nd ACM SIGKDD International Conference on Knowledge Discovery and Data Mining (KDD '16), San Francisco, CA, August 13−17, 2016*; Association for Computing Machinery: New York, NY, U.S.A., 2016; pp 785−794.
(43) Breiman, L. Random Forests. *Mach. Learn.* **2001**, *45*, 5−32.
(44) Ke, G.; Meng, Q.; Finley, T.; Wang, T.; Chen, W.; Ma, W.; Ye, Q.; Liu, T. Y. LightGBM: A Highly Efficient Gradient Boosting Decision Tree. In *Proceedings of the 31st International Conference on Neural Information Processing Systems (NIPS'17), Long Beach, CA, December 4−9, 2017*; Curran Associates, Inc.: Red Hook, NY, U.S.A., 2017, pp 3149−3157.

https://doi.org/10.1021/acs.langmuir.2c03465
Langmuir 2023, 39, 4984−4992